ECN-RX--06-052

The positive effect of NO on the N_2O decomposition activity of Fe-ZSM-5: A combined kinetic and in situ IR spectroscopic study

G. D. Pirngruber and J.A.Z. Pieterse

Journal of Catalysis, Volume 237, Issue 2, 25 January 2006, Pages 237-247

FBBRUARY 2006

Abstract

NO-assisted N_2O decomposition over four different Fe-ZSM-5 samples prepared by wet ion exchange (WIE) or chemical vapor deposition (CVD) of $FeCl_3$ was investigated by steady state kinetics, in situ IR spectroscopy and transient response methods. In spite of their lower iron loading, the samples prepared by wet ion exchange had the highest activity for N_2O decomposition in the presence of NO. The in situ IR experiments showed that the most active sample was characterized by a high concentration of adsorbed NO as well as adsorbed NO_2 under reaction conditions. Step response experiments proved that NO_2 is an intermediate of the catalytic cycle and functions as intermediate oxygen storage. IR and transient kinetic experiments show that WIE catalysts behave qualitatively different in NO assisted N_2O decomposition than CVD catalysts. These differences are discussed in terms of the different structure of the iron species in the two types of samples.

Keywords: Fe-ZSM-5, CVD, wet ion exchange, N_2O decomposition, NO, in situ IR, step response, pulse response

Introduction

N_2O emissions have a major contribution (6 %) to the global green house effect [1]. A considerable fraction of the total N_2O emissions are caused by the chemical industry, in adipic acid and nitric acid plants. Abatement of these emissions by catalytic decomposition of N_2O is an important issue. Noble metal catalysts have very high intrinsic activities for N_2O decomposition [2]. In the exhaust gas stream of adipic and nitric acid plants, however, N_2O is present together with NO and other components, like O_2, H_2O, etc. Most noble metal catalysts are strongly deactivated by the presence of these other components, in particular by NO [3,4]. Iron zeolites show the opposite behavior: Their N_2O decomposition activity is strongly enhanced by the presence of NO in the feed. This was originally attributed to a stoichiometric reaction of NO with N_2O, yielding N_2 and NO_2 [5]. Later, it was shown that NO has a truly catalytic effect on the N_2O decomposition activity [6]. Small amounts of NO increased N_2O conversion more than stoichiometrically. A redox mechanism with nitrites and nitrates as the redox species was given, but no spectroscopic evidence was provided.

$N_2O + *\text{-}NO_3^- \rightarrow *\text{-}NO_2^- + N_2 + O_2$ (1)

$N_2O + *\text{-}NO_2^- \rightarrow N_2 + *\text{-}NO_3^-$ (2)

Mul et al. [7] also observed that a small amount of NO led to an increase in the conversion of N_2O by significantly more than one N_2O per NO added (as would be the case for the stoichiometric reaction). The effect of NO was explained by a different model [8]: NO which is adsorbed on the catalyst reacts with the oxygen atom that N_2O deposits on the catalyst surface and forms adsorbed NO_2. Thereby, the site for the activation N_2O comes free again and a second oxygen atom from N_2O is deposited there. O_2 desorption occurs by recombination of the second deposited oxygen atom with an oxygen atom from NO_2. The reaction equations, which are given below, show that the role of NO in the cycle in purely catalytic. It functions as an intermediate storage for deposited oxygen atoms.

$* + N_2O \rightarrow *\text{-}O + N_2$ (3)

$*\text{-}O + *\text{-}NO \rightarrow * + *\text{-}NO_2$ (4)

$* + N_2O \rightarrow *\text{-}O + N_2$ (5)

$*\text{-}O + *\text{-}NO_2 \rightarrow * + *\text{-}NO + O_2$ (6)

Sum: $2\ N_2O \rightarrow 2\ N_2 + O_2$

The beneficial role of NO_2 in O_2 formation is reminiscent of mechanistic studies of NO decomposition over copper zeolites [9,10]. Also in this system it was found that NO_2 enhances the rate of O_2 formation by facilitating the recombination of two remote surface oxygen atoms via transport in the gas phase, i.e.

$$*\text{-O} + NO \rightarrow * + NO_2 \qquad (4a)$$

$$NO_2 + *\text{-O} \rightarrow * + NO + O_2 \qquad (6a)$$

This sequence is identical to the steps (4) and (6) in the scheme above, but NO_2 in the gas phase is involved instead of adsorbed NO_2.

In contrast, conventional N_2O decomposition occurs via the recombination of two deposited oxygen atoms on the surface, i.e.

$$2 * + 2\ N_2O \rightarrow 2\ *\text{-O} + 2\ N_2 \qquad (7)$$

$$2\ *\text{-O} \rightarrow O_2 \qquad (8)$$

The enhancement of the N_2O decomposition activity by NO depends on the relative rate of the two catalytic cycles. Recently, Pieterse et al. studied N_2O decomposition in the presence of NO, oxygen and water over Fe-ZSM-5 samples prepared by wet ion-exchange (WIE), sublimation (CVD) and steam-activated isomorphous substitution [11]. It was concluded that WIE resulted in catalysts with the highest N_2O conversion, although they contained much less iron than the CVD samples studied. It was proposed that the differences observed among the Fe-ZSM-5 samples prepared by the various methods are related to the ability of the predominant iron species to catalyze NO assisted N_2O decomposition. In order to explore this possibility in more detail, we studied the NO assisted N_2O decomposition over Fe-ZSM-5 samples, prepared by chemical vapor deposition or wet ion exchange, from two different parent zeolites. The beneficial effect of NO strongly differed from one sample to another. By combining characterization data, in situ IR spectroscopy and transient response measurements, we offer an explanation for that phenomenon. Furthermore, the mechanism of NO-assisted N_2O decomposition is discussed in detail.

Experimental

Sample preparation

Two parent ZSM-5 samples were used, i.e. MFI-P46 (Südchemie, Na-H-ZSM-5, Si/Al = 24, synthesized with template) and SM27 (Alsi Penta/Südchemie, NH_4-ZSM-5, Si/Al = 12, template-free synthesis). MFI-P46 was transformed in the NH_4-form by three-fold exchange with a 1M NH_4NO_3 solution. The NH_4 form of the samples was used for the chemical vapor deposition of $FeCl_3$ (CVD) [12] or for wet ion exchange

with an aqueous solution of $FeSO_4$. For CVD, the samples were first treated in O_2 at 773 K for 1 h, $FeCl_3$ was sublimed onto the zeolite at 593 K followed by extensive washing and another calcination at 773 K [13]. Wet ion exchange was carried out with $FeSO_4*7H_2O$ at 353 K for 6 h in N_2 atmosphere, to avoid oxidation of Fe^{2+} to Fe^{3+}. Exchange with Fe^{2+} ions is preferred over exchange with Fe^{3+} ions since Fe^{3+} ions tend to precipitate as Fe_2O_3 clusters on the outer surface of the zeolite. 1 mmol of iron was used in the exchange solution per gram of NH_4-ZSM-5, Si/Al 12, while 0.5 mmol of iron was used per gram of NH_4-ZSM-5, Si/Al 24. For filtration two times 1000 ml demiwater per 10 g cake was poured on the cake while keeping the cake under vacuum. The samples were subsequently dried in an oven at 353 K. The samples were calcined at 773 K during 5 hours (heating rate 1 K/min) in static air under shallow bed conditions. During the calcination oxidation of the exchanged Fe^{2+} ions to Fe^{3+} takes place. UV-Vis spectra of the calcined iron zeolites were recorded in diffuse reflection on a Cary 400 UV-Vis spectrometer equipped with a Praying Mantis sample stage from Harrick. The Fe and Al contents of the samples were determined by AAS, after dissolving the zeolites in HF and HNO_3 (see Table 1).
The samples are coded Fe-ZSM-5-x-CVD (WIE) where x stands for the Si/Al ratio of the parent and CVD or WIE for the preparation method.

Activity measurements

Catalytic tests were carried out in a computer-controlled multi-port flow set-up. Quartz reactors with an internal diameter of 5 mm were placed in a heated reactor vessel. The catalyst sieve fraction (0.25–0.5 mm) is placed on a quartz grid. Space velocities (GHSV) are reported at room temperature and atmospheric pressure. The feed consisted of 3000 ppm N_2O and 0 or 800 ppm NO, the balance being N_2. The purity of the used gases was 99% and 99.8% for N_2O and NO, respectively. The quantitative analysis of N_2O, N_2 and O_2 was performed using a micro-GC equipped with Poraplot and Molsieve columns and FID and TCD detectors. NO_x was analyzed with a NO_x (chemoluminescence) analyzer. At the start of each activity experiment, the reactor temperature was increased to 533 K at 3 K/min under N_2 flow and flushed for 3 h. Subsequently, the reaction gas mixture was fed to the catalyst. Preconditioning was set for 20 min at each temperature. Data was collected at ascending temperature using a ramp of 5 K/min to 773K at maximum.

In situ IR spectroscopy

6 mg sample were pressed into a self-supporting pellet of 6 mm diameter, placed in a gold sample holder and inserted into a cylindrical oven. The oven was screwed on a

stainless steel cell block equipped with gas connections and CaF_2 windows for letting the IR beam pass through cell and sample. The gas steam flows along the axis of the cylindrical oven through the sample pellet to the exit on the other side. Since the oven does not fill the whole cross section of the cell about 10% of the gas bypasses the sample, the rest flows through it. The cell represents a reasonable approximation of a plug flow reactor and is, due to its small volume, suited for fast switching from one gas mixture to another.

The samples were heated in a stream of 5% O_2 in He at 673 K, then kept for 30 min in a flow of pure He and cooled to reaction temperature (usually 573 K was chosen as initial temperature). The initial treatment in O_2 serves to remove hydrocarbon impurities, the subsequent treatment in He allowed for partial autoreduction of Fe^{3+} to Fe^{2+}. The reaction was started by switching from He to a mixture of 3000 ppm N_2O and 800 ppm NO in He. NO was purified with a cold trap at 173 K. The reaction was followed for 30 min by IR. The gas phase was simultaneously analyzed by GC and mass spectrometry. Then the feed was switched back to He. The temperature was raised to 673 K for 30 min and the procedure was repeated at the next temperature. The total gas flow through the cell was kept constant at 20 ml_{NTP}/min. For a pellet of 6 mg that corresponds to GHSV = 120000 h^{-1} (using a density of 0.5 g/ml).

The IR spectra were recorded on a Biorad FTS 3000 MX spectrometer equipped with a broad band MCT detector. The spectral resolution was 4 cm^{-1}. The catalyst pellet at the reaction temperature in a flow of He was used as background. The ZSM-5-12 samples were not very transparent, which had a negative effect on the signal to noise ratio. The corresponding spectra were Fourier filtered, in order to reduce the noise. The effluent of the IR cell was monitored by a Omnistar mass spectrometer. m/e values of 4, 28, 30, 32, 44 and 46 were recorded. All signals were normalized to the signal of He (m/e = 4) and the concentrations were calculated from a calibration matrix. The low sensitivity of the mass spectrometer for NO_2 did not allow us to obtain reliable NO_2 concentrations. The concentration of NO_2 can be inferred from the difference $c_{N2} – 2*c_{O2}$. That was verified by a few selected experiments with a NO_x analyzer.

Transient response measurements

50 mg of pelletized sample were placed in a quartz tube of 4 mm inner diameter and treated in a flow of He at 673 K for 1h. The reactor was cooled to 648 K and the feed was switched to 800 ppm NO in He. Pulses of 5000 ppm N_2O were given into the flow of NO, in an interval of ~100 s. Then, after letting the system reequilibrate for 10 min, a step to 3000 ppm N_2O in He was performed. The reaction was followed for

~30 min, the feed was stepped back to NO and finally once again to N_2O. The procedure was repeated at 673 K. The total flow rate in the experiments was 50 ml NTP/min, corresponding to GHSV = 30000 h^{-1}. The reaction products were analyzed by mass spectrometry, as described above.

Results

UV-Vis

The UV-Vis spectra of both WIE samples show only two intense ligand-to-metal charge transfer bands at 43000 cm^{-1} and 38000 cm^{-1}, as expected for isolated iron ions [14]. In the Fe-ZSM-5-24 CVD sample a shoulder appears at 27000 cm^{-1}, which indicates clustering of the iron atoms [15]. An absorption at 20000 cm^{-1} shows that some Fe_2O_3 particles are also present. In the UV-Vis spectrum of Fe-ZSM-5-12 CVD the band of Fe_2O_3 is more intense. The spectrum of Fe-ZSM-5-12 CVD differs from the others. It is dominated by two intense bands at 28000 and 43000 cm^{-1}. The position of the bands suggests an assignment to Cl→Fe charge transfer transitions [16], i.e. the chloride could not be completely removed during the repeated washing and calcination of that sample. It should be noted that the band at 28000 cm^{-1} was observed before on a Fe-ZSM-5-12 sample prepared from the same parent zeolite using a $FeCl_2$ precursor, but was, in our opinion, erroneously assigned to binuclear iron species [17].

IR spectroscopy

The IR spectra of the parent zeolites ZSM-5-12 and ZSM-5-24 show distinct differences. ZSM-5-24 has two intense bands in the region of the OH-stretching vibrations, at 3735 cm^{-1} (silanol groups) and at 3600 cm^{-1} (Brønsted OH groups). A very weak band at 3660 cm^{-1} is attributed to Al-OH groups on extraframework species. In the case of ZSM-5-12, the Brønsted OH-band is more intense, due to the higher Al concentration, and the silanol band is very weak. The two bands at 3735 and 3715 cm^{-1} are assigned to external and internal silanol groups [18]. After ion exchange, the intensity of the Brønsted-OH band decreases (see Table 1). In the ion-exchanged samples the fraction of exchanged OH groups corresponds to the Fe/Al ratio, i.e. one Fe atom is exchanged for one Brønsted site, as already observed for Cu^{2+} [19,20]. For reasons of charge balancing, the iron must be bound as $[Fe(OH)_2]^+$. If a dimer is formed, which bridges two ion exchange sites, charge balancing can also be achieved by $[OH\text{-}Fe\text{-}O\text{-}Fe\text{-}OH]^{2+}$ or by $[OH\text{-}Fe\text{-}\mu\text{-}(OH)_2\text{-}Fe\text{-}OH]^{2+}$. The vibration of the Fe-OH groups can be recognized as a broad band at 3660 cm^{-1} in the

spectra of both ion-exchanged samples (Figure 2). In the CVD samples, on average three iron atoms are bound to one Al sites, in the form of small iron oxide clusters. In earlier studies exchange degrees corresponding to roughly two iron atoms per Al were reported for the CVD method [21,22].

Comparison of catalytic activity

A comparison of the N_2O decomposition activity of the samples shows two trends (Figure 3): Si/Al = 12 > Si/Al = 24, and CVD > WIE. In essence, activity increases with the iron loading of the samples. Addition of NO changes the situation. The activity of the WIE samples is strongly boosted by NO and they become significantly more active than the CVD samples, in spite of their lower iron loading. For a semiquantitative description we compare the temperatures at which the catalysts reach a N_2O conversion of 20% (Table 2). Addition of NO shifts the activity curve by –100 K for the WIE samples and by –80 K and –60 K for the CVD samples with Si/Al = 24 and 12, respectively.

The NO concentration profile shows how NO influences the conversion of N_2O (Figure 4). When the temperature is raised the concentration of NO decreases and NO_2 is produced (not shown). NO_2 is not formed via reaction of NO with O_2, originating from decomposition of N_2O, but by direct reaction with N_2O [8], i.e.

$$NO + N_2O \rightarrow NO_2 + N_2 \qquad (9).$$

Most of the N_2O conversion in temperature range 550 – 650 K is due to this stoichiometric reaction of NO with N_2O (see Figure 5). Above ~ 650 K, the effect of NO becomes mainly catalytic. N_2O decomposition strongly increases and the NO concentration increases again.

In situ IR spectroscopy

In order to explain the different activity of the four samples based on the nature and concentration of adsorbed surface species, in situ IR spectroscopy was used. Thin catalyst pellets were exposed to a flow of 3000 ppm N_2O and 800 ppm NO in He. The space velocity in these experiments was a factor of two lower than in the activity measurements described above. The adsorbed species were characterized in the temperature range of 573 to 648 K, i.e. in the range where first the stoichiometric and then the catalytic reaction between NO and N_2O sets on.

Figure 6 shows the time evolution of the spectra measured for Fe-ZSM-5-24 WIE at 573 K. A nitrosyl band at 1878 cm^{-1} increased rapidly, in parallel with the concentration of NO in the gas phase. After 4 min, the nitrosyl band reached its maximum intensity and then slightly decreased. A band at 1623 cm^{-1} increased

gradually with time. According to its wavenumber, this band can be assigned to a nitrato (NO_3^-) or a weakly bound nitro group (NO_2) [23,24]. The band disappeared rapidly when switching from the reaction mixture to He. We therefore assign the band to a weakly bound NO_2 species [25] rather than to a NO_3^- group, which would have a higher thermal stability. The appearance of the nitro band indicates that oxidation of NO to NO_2 took place. As expected from the stoichiometry of reaction 9 a higher concentration of N_2 was observed in the gas phase during the build up of NO_2 on the surface.

The doublets at 3498/ 3464 cm^{-1}, at 2583/2547 cm^{-1} and at 2238/2208 cm^{-1} are due to gas phase N_2O. A low frequency tail of the 2208 cm^{-1} band can be attributed to NO^+ species, but its concentration is much lower than in a feed of NO + O_2 [26]. Also in the high-frequency region of the spectrum new bands emerged. The most intense band was a doublet at 3660 and 3630 cm^{-1} (Figure 6). These bands were observed before during reaction of N_2O with Fe-ZSM-5 and were assigned to a $Fe(OH)_2$ group [27]. They are generated during the oxidation of Fe^{2+} to Fe^{3+} [28]. The source of the additional OH-groups must be traces of water in the feed. The OH-bands do not appear when only NO is flown over the catalyst.

Figure 7 compares the spectra of the four investigated catalysts in the region of the relevant NO_x vibrations. The two WIE samples exhibit a more intense nitrosyl band than the two CVD samples. The intensity of the nitro band is similar on all catalysts. On Fe-ZSM-5-12 WIE an additional broad absorption can be found at ~1500 cm^{-1}. The wavenumber suggests assignment to a surface nitrito species, i.e. a -O-N=O^- group bound to surface via the oxygen atom [23]. The band did not disappear when switching to He, which supports the assignment to a strongly bound charged species. The CVD samples exhibit a weak band at 1530 cm^{-1}. The band had a high thermal stability and must therefore be due to a charged species (nitrito or nitrato), but it could not be exactly assigned. $Fe(OH)_2$ bands at 3660 and 3630 cm^{-1} are found on both catalysts prepared by WIE (not shown). On the CVD samples only a broad band due to hydrogen bonded hydroxyls appears instead, due to the higher density of iron sites on the CVD materials.

A control experiment with the parent ZSM-5-12 sample (600 ppm Fe) yielded entirely different spectra. No new OH-stretching vibrations were observed. A weak nitrosyl band was formed, due to adsorption of NO on the Fe impurities or on Al^{3+} [29], but the intensity of the nitrosyl band was ten times weaker than on Fe-ZSM-5-12 WIE. Further, a multitude of bands was formed between 1800 and 1300 cm^{-1}, attributed to surface nitro, nitrato and nitrito groups. These bands were highly stable on the catalyst surface and behaved like spectators when switching from the reaction

mixture to He and back. The behavior of the parent is completely different to the CVD and WIE samples. Activity tests in the plug flow reactor showed that the activity of the parent sample was negligible compared to Fe-ZSM-5. We can, therefore, state that (a) the catalysis runs on the iron cations (clusters), which were introduced by exchange, and that (b) the in situ IR measurements probe the adsorption/reaction on these iron sites and not on the zeolite matrix.

At 623 K the adsorbed species on Fe-ZSM-5 reached steady state much quicker than at 573 K (not shown). The intensity of the nitrosyl bands at 1880 cm^{-1} stabilizes at a value that is approximately a factor of five lower than at 573 K (see Figure 8a). The intensity of the NO_2 band, on the other hand, increases for the two WIE samples and remains roughly constant for Fe-ZSM-5-24 CVD. Due to the high noise level of the spectrum, Fe-ZSM-5-12 CVD is not included in the comparison. In addition to the nitrosyl and nitro band, Fe-ZSM-5-12 WIE exhibits additional absorptions at 1570 and at 1500 cm^{-1}. In analogy to Cu-ZSM-5, the former band can be assigned to chelating nitrate species (see Scheme 1) [30,31]. The latter is due to nitrite species (*vide supra*).

When switching from the reaction mixture back to He the nitrosyl band disappeared very quickly (in parallel with the decrease of the NO concentration in the gas phase). In the case of Fe-ZSM-5-12 WIE, also the nitro band disappeared within a few minutes. For the other catalysts, a fast initial decrease of the nitro band was observed, but a band at 1630 cm^{-1} remained and decreased only very slowly with time. This shows that the nitro groups on Fe-ZSM-5-12 WIE are very labile whereas part of the surface nitro groups on the other catalysts have a rather high thermal stability.

At 648 K the nitrosyl band decreases further in intensity compared to 623 K (see Figure 8b). The intensity of the nitro band increases for the sample Fe-ZSM-5-12 WIE and slightly decreases for the other samples. The intensity of the NO_2 band at 648 K follows the order Fe-ZSM-5-12 WIE > Fe-ZSM-5-24 WIE > Fe-ZSM-5-24 CVD > Fe-ZSM-5-12 CVD. The same order is also obtained at 623 K if only the labile nitro groups are counted (i.e. those which desorb within 1 min in He). Note that the intensity of the nitrosyl band at lower temperatures (573 K) follows the same order.

The N_2O conversions measured in the in situ IR experiments were approximately a factor of 10 lower than in the plug flow reactor. At 573 K hardly any measurable activity was observed in the IR cell, at 648 K conversions ranged from 2 to 7%.

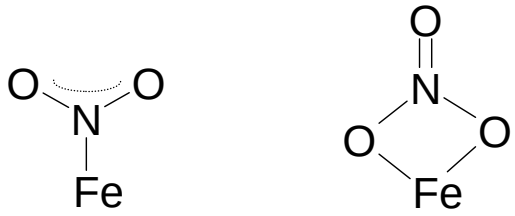

1625 cm^{-1} 1575 cm^{-1}

Scheme 1 Structures of adsorbed NO_2 and of chelating nitrate.

Pulse and step experiments

In order to obtain more insight into the reactivity of the surface species pulse and step experiments were carried out. These experiments were performed in a tubular quartz reactor, at 648 and 673 K, and in the IR reactor, at 648 K. In the IR reactor the space velocity was roughly a factor of four lower than in the plug flow reactor.

When N_2O was pulsed into a flow of NO over the catalyst Fe-ZSM-5-12 WIE a peak of N_2 was formed (see Figure 9). A peak of O_2 was detected at 673 K, but not at 648 K. The O_2 peak strongly tailed with respect to N_2 peak. The same phenomenon was observed in earlier TAP experiments [8]. In the IR reactor the nitrosyl band at 1880 cm^{-1} decreased during the N_2O pulse and restored its original intensity after the pulse, i.e. some NO was replaced by the incoming N_2O. Nitro bands were not detected. It is interesting to note that the pulse of N_2O was strongly broadened and tailed, especially at 648 K. This indicates that some N_2O was molecularly adsorbed on the iron sites. The effect was observed on both WIE catalysts, but not on Fe-ZSM-5-24 CVD. Fe-ZSM-5-24 CVD also did not produce any O_2 during the N_2O pulses, even at 673 K.

After the pulses of N_2O, a step from NO to N_2O was performed (see Figure 10). A peak of N_2 was produced right after the step. The peak of N_2 is not related to NO_2 formation, but is due to the reoxidation of Fe^{2+} sites to Fe^{3+} [32]. NO was desorbed from the catalyst (indicated by the peak of NO in Figure 10b), being replaced by N_2O. With some delay the production of O_2 set in. After 40 s, N_2 and O_2 decayed in parallel to the steady-state value. The steady state activity is due to NO-unassisted N_2O decomposition.

The delayed onset of O_2 formation, followed by the simultaneous decay of N_2 and O_2 were also observed in the IR reactor (Figure 11). Due to the higher space velocity, less O_2 was formed. The intensity of the surface nitrosyl band decreased in parallel with the gas phase concentration of NO. A desorption peak of NO, as in the tubular

quartz reactor, was not observed, again due to the high space velocity. With a delay of ~10 s (similar to the delay of O_2 formation), a nitro band was formed. The nitro band increased in intensity as long as NO was still present in the gas phase and then slowly decreased. Figure 11 shows that the evolution of the NO_2 band and the formation of O_2 in the gas phase were synchronized.

The behavior of the other catalysts was only studied in the tubular quartz reactor. Fe-ZSM-5-24 WIE behaved qualitatively like Fe-ZSM-5-12 WIE, but its activity for O_2 formation after the step was lower (Table 3). With Fe-ZSM-5-24 CVD no accelerated O_2 formation could be observed. The activity settled immediately at its steady value, due to unassisted N_2O decomposition.

After the step back from N_2O to NO, a small peak of O_2 and an even smaller peak of N_2 was observed. The O_2 formation decayed in less than 80 s. The amount of O_2 formed decreased from Fe-ZSM-5-12 WIE (0.015 mol/mol Fe) to Fe-ZSM-5-24 WIE (0.008 mol/mol Fe) and Fe-ZSM-5-24 CVD (0.001 mol/mol Fe). In the IR reactor a nitro band increased and decayed simultaneously with the O_2 peak.

Discussion

The structure of the iron sites in WIE and CVD catalysts

The UV-Vis and IR spectra suggest that the WIE samples contain isolated iron cations located at ion exchange positions. Recent EXAFS data indicate, however, that iron dimers can be formed at high ion exchange degrees [33], as already reported for Cu-ZSM-5 [34]. Since the Fe/Al ratio of our WIE samples is rather high (Fe/Al = 0.26 and 0.45) we expect that a mixture of isolated sites and dimers is present. In case of the CVD samples, several studies have shown that they contain small oligomeric iron oxide clusters [35-37]. This is confirmed by the UV-Vis and IR data presented here.

The adsorbed species

The dominating surface species in our experiments are mononitrosyl species (1880 cm^{-1}) and adsorbed NO_2 (1625 cm^{-1}). Both bands were also observed in the IR study by Mul et al. [7], which was, however, performed at lower temperatures. The stretching frequency of the nitrosyl band is only slightly higher than the stretching frequency of NO in the gas phase (1876 cm^{-1}), indicating a very weak coordinative bond of NO to iron. When NO adsorption is studied at room temperature a multitude of bands, assigned to di- and trinitrosyl species [38] or to mononitrosyls adsorbed in different positions in the ZSM-5 host [39], is observed. At the high temperatures

employed in our in situ experiments NO does not discriminate between these sites and only a single band is observed. It is generally agreed that NO adsorbs rather strongly on Fe^{2+}, but only weakly or not at all on Fe^{3+} [23,38]. Test experiments confirmed that catalysts, which were not allowed to autoreduce in He before switching to the reaction mixture, adsorbed less NO. We therefore assign the band at ~1880 cm^{-1} to mononitrosyl species bound to Fe^{2+} [40].

The second prominent band in the spectra is the nitro band at 1625 cm^{-1}. In case of the Fe-ZSM-5-12 WIE sample, the band exhibited a shoulder at 1575 cm^{-1} at higher temperatures. A similar pair of bands at 1625 and 1575 cm^{-1} is observed when NO + O_2 is passed over a Fe-ZSM-5 catalyst [25,41]. When formed from NO + O_2, the band at 1625 cm^{-1} has a rather high thermal stability and is probably due to a bridging nitrate species rather than an adsorbed nitro group. The two groups vibrate at very similar wavelength and can only be distinguished based on their thermal stability. At high concentrations (< 1%), bands at 1625 and 1575 cm^{-1} can also be formed from N_2O [42,43]. In the concentration and temperature range used in our study, however, N_2O does not create any strongly IR absorbing surface species [44]. The origin of the nitro/nitrate bands at 1625 cm^{-1} and 1575 cm^{-1} in our experiments must therefore be the oxidation of NO by N_2O. These bands are also formed upon reaction of NO + O_2 on our catalysts, but intensity and thermal stability is different.

The role of the surface species in the reaction mechanism

Two different models have been proposed to explain the catalytic effect of NO on N_2O decomposition, one involving nitrito and nitrato species [6], the other involving adsorbed NO_2, which functions as an intermediate oxygen storage [7,8]. In our in situ IR experiments, bands of adsorbed NO_2 (~1625 cm^{-1}), chelating nitrates (1575 cm^{-1}) and weak bands of nitrito species were observed. The band of molecularly adsorbed NO_2 was by far the most intense and its intensity at high temperatures correlated with the catalytic activity of the samples (Figure 12). During the step experiments, i.e. during a step from NO to N_2O, the NO_2 band appeared as the only new surface species and its intensity correlated with the O_2 formation. These three results prove that adsorbed NO_2 is indeed part of the catalytic cycle of NO assisted N_2O decomposition, as proposed by Perez-Ramirez et al. [8]. We return later to the question whether the chelating nitrate (1575 cm^{-1}) also plays a role in the reaction mechanism.

With the help of our transient response experiments we can extract more details of the catalytic cycle described in equations 3 to 6. When N_2O was pulsed into a flow of NO, we observed that unreacted N_2O was rather strongly retained on the WIE

catalysts, i.e. it was molecularly adsorbed (Figure 9). After a step of NO to N_2O, N_2O partly replaced NO from the adsorption sites, leading to the peak of NO observed in Figure 10b. The two pieces of information suggest that N_2O adsorbs molecularly on the WIE catalysts and that N_2O competes with NO for adsorption sites. After the step from N_2O to NO, NO_2 species were only formed as long as N_2O was still present in the gas phase. We therefore propose that, instead of adsorbed oxygen atoms, molecularly adsorbed N_2O is involved in the formation of NO_2 on the WIE catalysts. We can write the reaction mechanism as

$$Fe^{2+}(NO) + N_2O \rightarrow Fe^{2+}(NO)(N_2O) \rightarrow Fe^{2+}(NO_2) + N_2 \qquad (11)$$

$$Fe^{2+}(NO_2) + N_2O \rightarrow Fe^{2+}(NO) + N_2 + O_2 \qquad (12)$$

After the step from NO to N_2O, N_2O replaces NO from adsorption sites, as also observed by Mul et al. [7]. Then NO_2 is formed by reaction of adsorbed NO with N_2O (reaction 11), which is adsorbed on the same or on a neighboring iron site (if the iron sites are dimers). The concentration of adsorbed NO_2 reaches its maximum when the gas phase NO concentration decreases to zero. After that the build-up of NO_2 by reaction 11 ceases and only it consumption by reaction 12 follows. Reaction 12 should restore adsorbed NO on the surface. Adsorbed NO was, however, not observed any more 50 s after the step to N_2O (Figure 11). The reason is that adsorbed NO, once regenerated by reaction 12, is rapidly reoxidized to NO_2 by reaction 11. The consumption of NO_2 by reaction 12, on the other hand, is slow. Also earlier work concluded that O_2 formation is the rate limiting step of the reaction [7,8]. Instead of being oxidized to NO_2 and refed to the catalytic cycle, the adsorbed NO can also desorb into the gas phase. This process terminates the catalytic cycle and leads to the slow decay of the catalytic activity when NO is not present in the feed. The competition between oxidation of NO to NO_2 and its desorption from the surface determines how much O_2 can be formed after the step from NO to N_2O.

In contrast to the WIE samples, enhanced N_2 formation after the step from NO to N_2O was not observed for the CVD catalyst (see Table 3). The replacement of adsorbed NO by N_2O, resulting in a desorption peak of NO, was also not observed. We presume that, on the CVD catalyst, N_2O adsorbs and dissociates on sites, which are remote from the NO adsorption sites. The deposited oxygen atom has to migrate to the adsorbed NO in order to form NO_2. This process is slower than the direct reaction of adsorbed NO with N_2O on the WIE catalysts. Hence, significant amounts of NO_2 are not formed in the step experiment with the CVD catalyst and enhanced N_2 formation is not observed. Note, however, that NO_2 formation is not the rate limiting

step in steady state. The slower NO_2 formation on the CVD catalysts can therefore not explain their lower activity in NO assisted N_2O decomposition.
It is worthwhile to analyze the O_2 formation (reaction 12), which is rate determining, in more detail. Different mechanistic pathways can be considered.

Option 1

$$Fe^{2+}(NO_2) + N_2O \rightarrow Fe^{2+}(NO_2)(N_2O) \rightarrow Fe^{2+}(NO) + N_2 + O_2 \qquad (12a)$$

Option 2

$$N_2O + Fe^{2+} \rightarrow Fe\text{-}O + N_2$$
$$Fe\text{-}O + Fe^{2+}(NO_2) \rightarrow Fe^{2+}(NO) + O_2 \qquad (12b)$$

Option 3

$$N_2O + Fe^{2+} \rightarrow Fe\text{-}O + N_2$$
$$Fe^{2+}(NO_2) \rightarrow Fe^{2+} + NO_2$$
$$Fe\text{-}O + NO_2 \rightarrow Fe\text{-}O(NO_2) \rightarrow Fe^{2+}(NO) + O_2 \qquad (12c)$$

Scheme 2 Possible mechanisms for the formation of N_2 and O_2 from reaction of NO_2 with N_2O

The first option is a direct reaction of N_2O with adsorbed NO_2, possibly via an intermediate where both molecules are adsorbed on the same iron site [45]. Alternatively, N_2O may first dissociate into N_2 and an adsorbed oxygen atom. If the oxygen atom is deposited in the vicinity of adsorbed NO_2 or if it has the possibility to migrate there it can react with NO_2 to give O_2 and adsorbed NO (reaction 13b). This is in essence the mechanism proposed by Perez-Ramirez et al. [8]. A third possibility is that NO_2 desorbs into the gas phase and reacts with an oxygen atom deposited from N_2O. The band at 1575 cm^{-1} can be tentatively ascribed to the intermediate formed between the deposited surface oxygen atom and a gas phase NO_2 molecule (see Scheme 1), which then decomposes to NO and O_2. A similar role of transporting oxygen atoms between distant sites to facilitate O_2 formation was attributed to NO_2 in the decomposition of NO over Cu-ZSM-5 [9,10]. Note that the first and the last pathway can operate on isolated iron sites whereas the second one requires the presence of two iron sites for the adsorption of oxygen and of NO/NO_2, which are located near to each other, i.e. a dimer or even larger iron cluster.
Can we decide whether the contribution of adsorbed NO_2 or of gas phase NO_2 dominates on the iron zeolites? Perez-Ramirez et al. [8] showed that when NO and N_2O were alternately pulsed over the catalyst at 773 K, NO_2 appeared in the gas phase only during the NO pulses, but O_2 was formed after the pulses of N_2O, i.e.

when NO_2 was not present in the gas phase. That speaks in favor of adsorbed NO_2. Our results show that the activity of the catalysts is correlated to the concentration of adsorbed NO_2 at 648 K. One has to keep in mind, however, that at 648 K the effect of NO/NO_2 on N_2O decomposition is still mainly stoichiometric and not catalytic. The catalytic effect of NO becomes more dominating at higher temperatures. Under these conditions we can expect that the adsorption of NO_2 on the surface is weak and the gas phase mechanism will certainly gain in importance.

Comparison of CVD and WIE samples

The IR measurements at 573 K correspond to a situation where conversion is close to zero. The concentration of adsorbed NO under these conditions correlates with the activity of the samples at higher temperatures (Figure 12). NO adsorbs preferentially on Fe^{2+}. The concentration of Fe^{2+} on the samples can be estimated from the initial peak of N_2, which was always observed in the step experiments. The peak of N_2 is related to reoxidation of Fe^{2+} to Fe^{3+}, according to the equation

$2Fe^{2+} + N_2O \rightarrow 2Fe^{3+} + O^{2-} + N_2$ (13).

We chose the values obtained in the steps from NO to N_2O (see Table 3) - the numbers are more precise than those of in the in situ IR experiments – and used the Fe^{2+}/N_2 stoichiometry of reaction 13. The concentration of Fe^{2+} determined by this method correlates with the concentration of adsorbed NO (Figure 13). At higher temperatures, i.e. with increasing N_2O conversion, an increasing fraction of adsorbed NO is converted into adsorbed NO_2. The more NO is adsorbed on the catalyst under non-reactive conditions, the more can be converted to NO_2 at higher temperatures (Figure 12) and thereby contribute to the increase in catalytic activity.

The addition of NO to the feed enhances the N_2O decomposition activity of the WIE catalysts more than of the CVD samples. Figure 13 shows that the WIE samples have a significantly higher concentration of Fe^{2+} than the CVD samples, in spite of the higher iron loading of the latter. Ion exchanged samples autoreduce more readily than catalysts prepared by CVD [46]. The higher concentration of Fe^{2+} leads to a higher concentration of adsorbed NO/NO_2 on the WIE samples and explains why WIE samples are more active in NO-assisted N_2O decomposition than CVD materials. A second reason may be the contribution of gas phase NO_2, which allows oxygen atoms that were deposited on distant iron sites to recombine (see option 3 in Scheme 2). Gas phase NO_2 is therefore expected to lead to a stronger enhancement of the reaction rate on isolated iron sites as compared to clustered iron sites where O_2 recombination is also possible via migration over the cluster.

In addition to the comparison WIE vs. CVD it is interesting to discuss the role of the parent zeolite. Fe-ZSM-12-WIE was by far more active than the analogous sample prepared from ZSM-5-24. In first instance, this can be explained by the higher iron loading of the former sample (see Table 1). If activity is normalized by the iron loading the two samples are similar. The high activity of Fe-ZSM-12 WIE is therefore mainly due to the high ion-exchange capacity of the sample, which allows for stabilizing a high concentration of isolated iron ions or dimers.

Conclusions

NO assisted N_2O decomposition was studied over Fe-ZSM-5 samples, prepared by two different methods, chemical vapor deposition and wet ion-exchange, from two different parent zeolites. Transient kinetic and IR experiments provide direct proof that adsorbed NO_2 is part of the catalytic cycle of NO assisted N_2O decomposition. The mechanism of NO_2 formation is different on WIE and CVD samples. On WIE catalysts NO_2 is formed by the direct reaction of adsorbed NO with N_2O on an isolated iron site or dimer. On CVD samples, containing oligomeric iron species, we presume that NO and N_2O adsorb on distant sites. NO_2 formation is significantly slower. NO_2 formation is, however, not the rate limiting step of the reaction. O_2 formation, although strongly accelerated compared to unassisted N_2O decomposition, is still the slowest step of the reaction sequence. O_2 is formed by the reaction of N_2O with adsorbed and/or gas phase NO_2. The involvement of gas phase NO_2 is expected to lead to a strong increase in the O_2 formation rate in catalysts containing isolated iron sites because it facilitates the recombination of oxygen atoms deposited on distant sites. This effect partly explains why WIE samples become more active in NO assisted N_2O decomposition than the CVD catalysts although the opposite sequence is found in the decomposition of pure N_2O. The main reason for the higher activity of the WIE samples is, however, a different one: WIE samples contain a higher concentration of Fe^{2+} sites under reaction conditions. NO preferentially adsorbs on Fe^{2+} and the concentration of Fe^{2+} determines how many sites take part in the NO assisted N_2O decomposition cycle.

Acknowledgements

Pijus K. Roy (ETH), Saskia Booneveld and Ruud van den Brink (ECN) are thanked for help with characterization of the samples and discussions.

Tables

Table 1 Elemental composition of the samples and fraction of the Brønsted OH groups exchanged against Fe, as determined by IR spectroscopy.

Sample	wt% Fe	Fe/Al	OH exchange
Fe-ZSM-5-24 WIE	1.0	0.26	0.25
Fe-ZSM-5-24 CVD	4.4	1.1	0.38
Fe-ZSM-5-12 WIE	2.8	0.45	0.47
Fe-ZSM-5-12 CVD	5.4	0.87	0.34

Table 2 Temperature at which the catalysts reach a N_2O conversion of 20%. Feed concentration 3000 ppm N_2O, 0 or 800 ppm NO, GHSV = 60000 h^{-1}.

	with NO	without NO	diff
Fe-ZSM-5-12 WIE	331	432	-101
Fe-ZSM-5-24 WIE	350	451	-101
Fe-ZSM-5-12 CVD	360	422	-62
Fe-ZSM-5-24 CVD	367	447	-80

Table 3 Quantification of the initial peak of N_2 formed after a step from 800 ppm NO to 3000 ppm N_2O in He, at 648 or 673 K, as well as of the amount of O_2 formed in the subsequent N_2O decomposition. GHSV = 30000 h^{-1}.

	N_2 peak	O_2 [a]	N_2 peak	O_2 [a]
648 K	μmol	μmol	mol/mol Fe	mol/mol Fe
Fe-ZSM-5-12-WIE	3.7	15	0.15	0.59
IR reactor[b]			0.14	0.07
Fe-ZSM-5-24-WIE	1.9	2.0	0.22	0.23
Fe-ZSM-5-24-CVD	0.7	0	0.02	0
673 K				
Fe-ZSM-5-12-WIE	1.21	21	0.05	0.85
Fe-ZSM-5-24-WIE	0.9	4.7	0.11	0.54
Fe-ZSM-5-24-CVD	0.5	0	0.01	0

[a] steady state activity, due to NO-unassisted N_2O decomposition, subtracted

[b] GHSV ~ 120000 h^{-1}

Figure Captions

Figure 1 UV-Vis spectra of Fe-ZSM-5-12/24 CVD and WIE.

Figure 2 IR spectra of the dehydrated samples measured at 523 K. (a) ZSM-5-12 parent (solid), WIE (dash), CVD (dotted), (b) ZSM-5-24 parent (solid), WIE (dash), CVD (dotted).

Figure 3 N_2O decomposition activity of the samples. Feed 3000 ppm N_2O, 0 or 800 ppm NO (full and open symbols), balance N_2, GHSV = 60000 h^{-1}. ZSM-5-12 WIE (squares), ZSM-5-24 WIE (diamonds), ZSM-5-12 CVD (triangles), ZSM-5-24 CVD (circles).

Figure 4 NO concentration profile. Feed 3000 ppm N_2O, 800 ppm NO, balance N_2, GHSV = 60000 h^{-1}. ZSM-5-12 WIE (squares), ZSM-5-24 WIE (diamonds), ZSM-5-12 CVD (triangles), ZSM-5-24 CVD (circles).

Figure 5 Conversion of N_2O vs. conversion of NO. Solid line corresponds to a conversion of one N_2O per NO. Fe-ZSM-5-12 WIE, GHSV = 60000 cm^{-1}.

Figure 6 Time evolution of IR spectra of adsorbed species on Fe-ZSM-5-24 WIE at 573 K during reaction with 3000 ppm N_2O and 800 ppm NO. Fe-ZSM-5-24 Spectra after 30 s, 1 min, 2 min, 4 min and 19 min (each offset by 0.002). GHSV = 120000 h^{-1}.

Figure 7 IR spectra after 30 min in 3000 ppm N_2O + 800 ppm NO at 573 K.

Figure 8 IR spectra after 30 min in 3000 ppm N_2O + 800 ppm NO at (a) 623 K and (b) 648 K.

Figure 9 Pulses of 5000 ppm N_2O into a flow of 800 ppm NO at (a) 648 K and (b) 673 K. Fe-ZSM-5-12 WIE, GHSV = 30000 h^{-1}.

Figure 10 (a) Step from 800 ppm NO to 3000 ppm N_2O in He at 648 K and step back to NO. (b) Zoom of the first 500 s after the step. Fe-ZSM-5-12 WIE, GHSV = 30000 h^{-1}.

Figure 11 Step from 800 ppm NO to 3000 ppm N_2O in He at 648 K in the IR reactor. Intensity of the nitrosyl band (circles) and of the NO_2 band (x 5, squares) on right axis. Gas phase concentration of N_2 (solid), NO (dotted), and O_2 (x 2, dashed). Fe-ZSM-5-12 WIE, GHSV ~120000 h^{-1} .

Figure 12 Intensity of the nitrosyl band at 1880 cm^{-1} at 573 K and of the nitro band at 1623 cm^{-1} at 648 K vs. the N_2O conversion at 648 K (in the IR reactor, i.e. at GHSV ~ 120000 h^{-1}).

Figure 13 Normalized intensity of the NO band at 1880 cm^{-1} obtained in the IR experiments at 573 K (normalized by thickness of pellet) vs. concentration of Fe^{2+} sites (values derived from Table 3, 648 K).

Figures

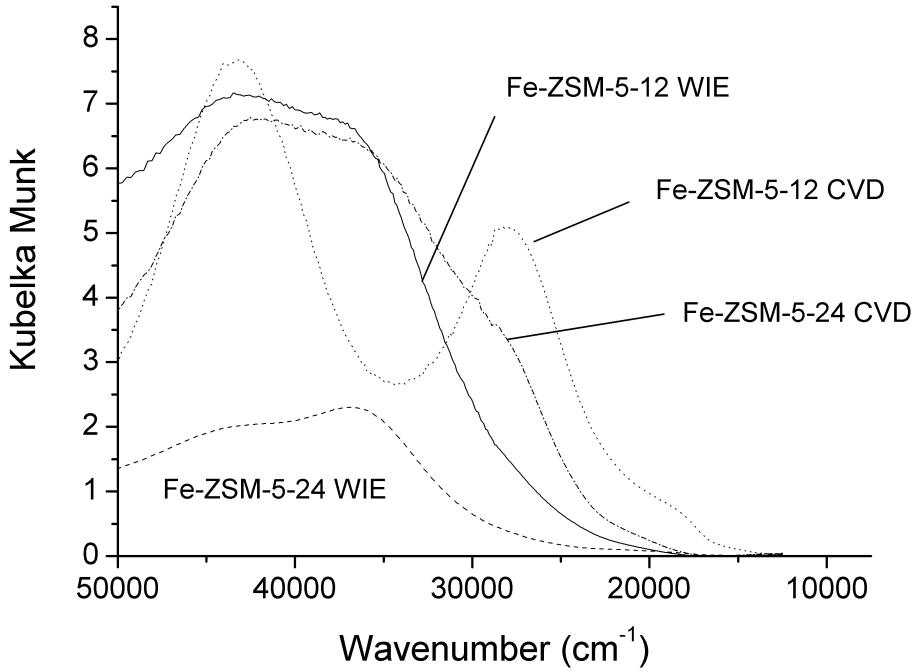

Figure 15 UV-Vis spectra of Fe-ZSM-5-12/24 CVD and WIE.

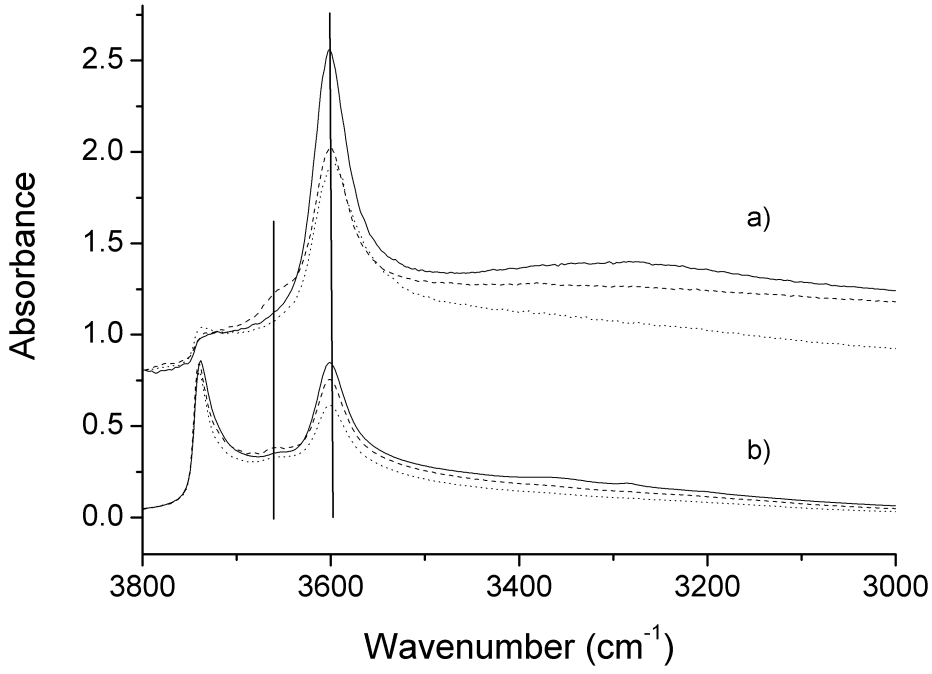

Figure 16 IR spectra of the dehydrated samples measured at 523 K. (a) ZSM-5-12 parent (solid), WIE (dash), CVD (dotted), (b) ZSM-5-24 parent (solid), WIE (dash), CVD (dotted).

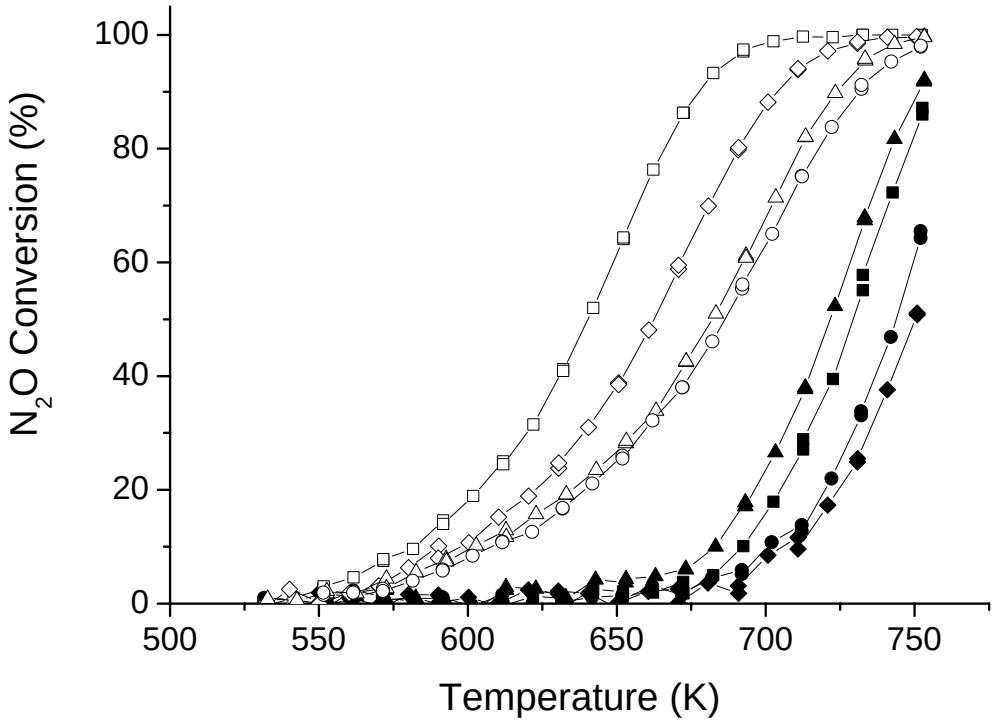

Figure 17 N_2O decomposition activity of the samples. Feed 3000 ppm N_2O, 0 or 800 ppm NO (full and open symbols), balance N_2, GHSV = 60000 h^{-1}. ZSM-5-12 WIE (squares), ZSM-5-24 WIE (diamonds), ZSM-5-12 CVD (triangles), ZSM-5-24 CVD (circles).

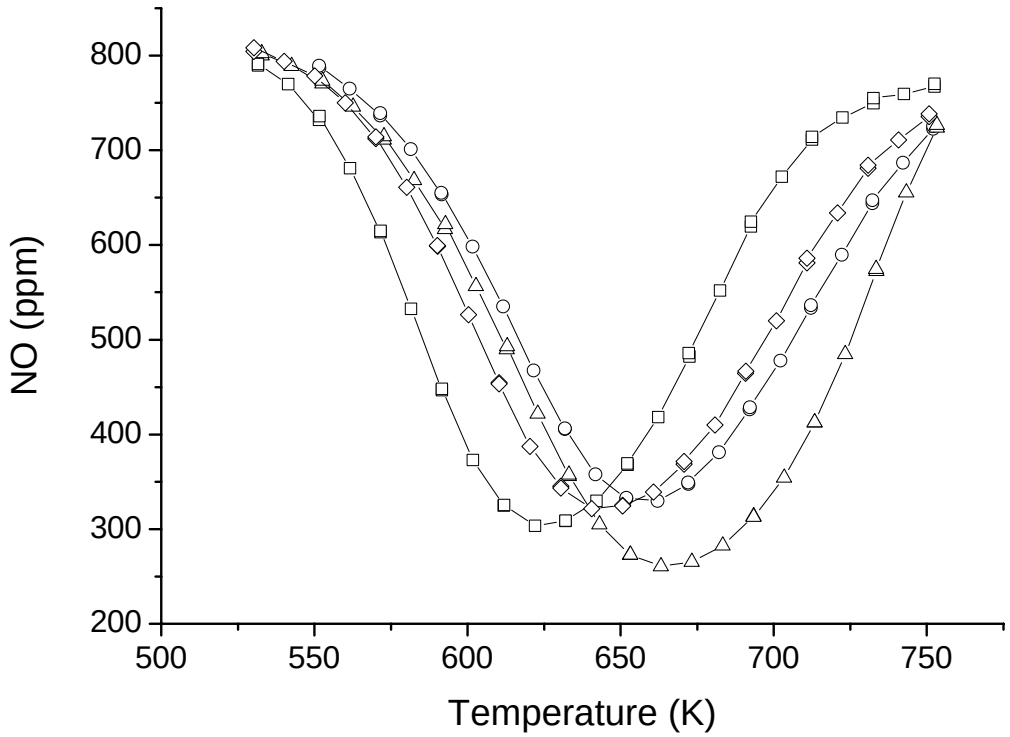

Figure 18 NO concentration profile. Feed 3000 ppm N_2O, 800 ppm NO, balance N_2, GHSV = 60000 h^{-1}. ZSM-5-12 WIE (squares), ZSM-5-24 WIE (diamonds), ZSM-5-12 CVD (triangles), ZSM-5-24 CVD (circles).

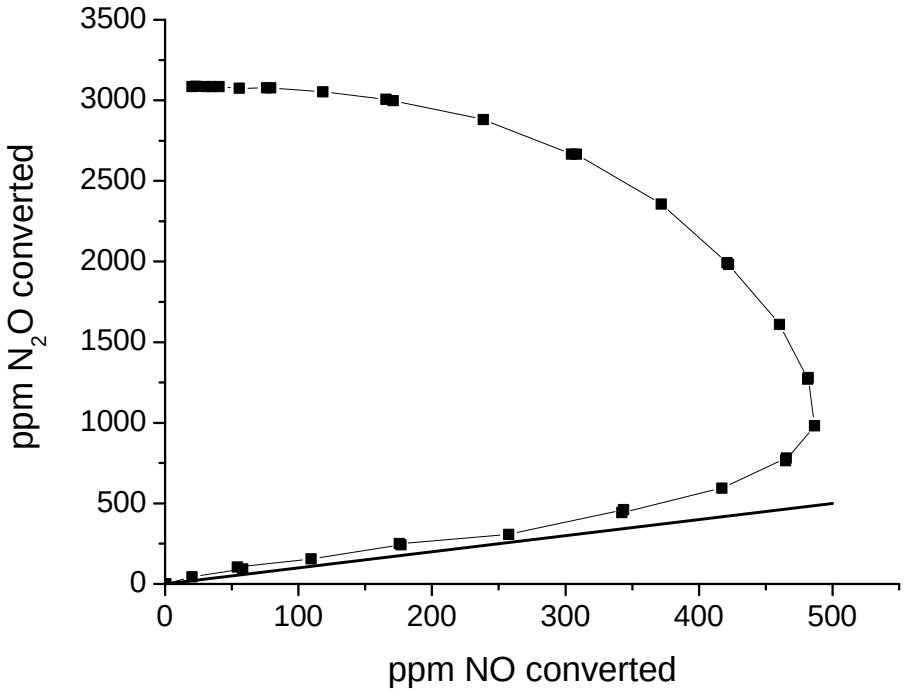

Figure 19 Conversion of N_2O vs. conversion of NO. Solid line corresponds to a conversion of one N_2O per NO. Fe-ZSM-5-12 WIE, GHSV = 60000 cm^{-1}.

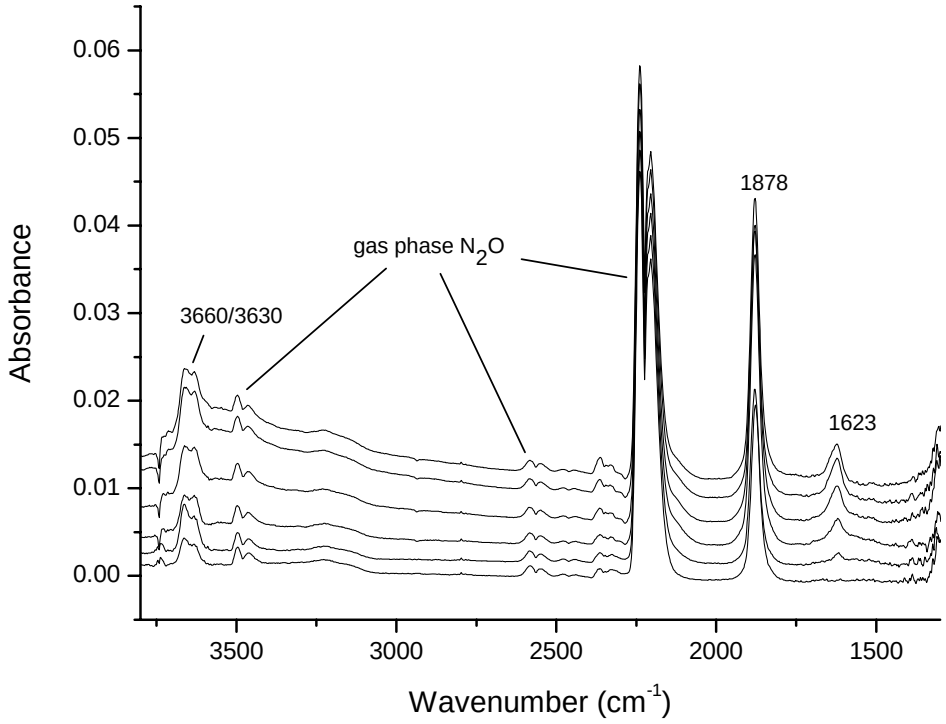

Figure 20 Time evolution of IR spectra of adsorbed species on Fe-ZSM-5-24 WIE at 573 K during reaction with 3000 ppm N_2O and 800 ppm NO. Fe-ZSM-5-24 Spectra after 30 s, 1 min, 2 min, 4 min and 19 min (each offset by 0.002). GHSV = 120000 h^{-1}.

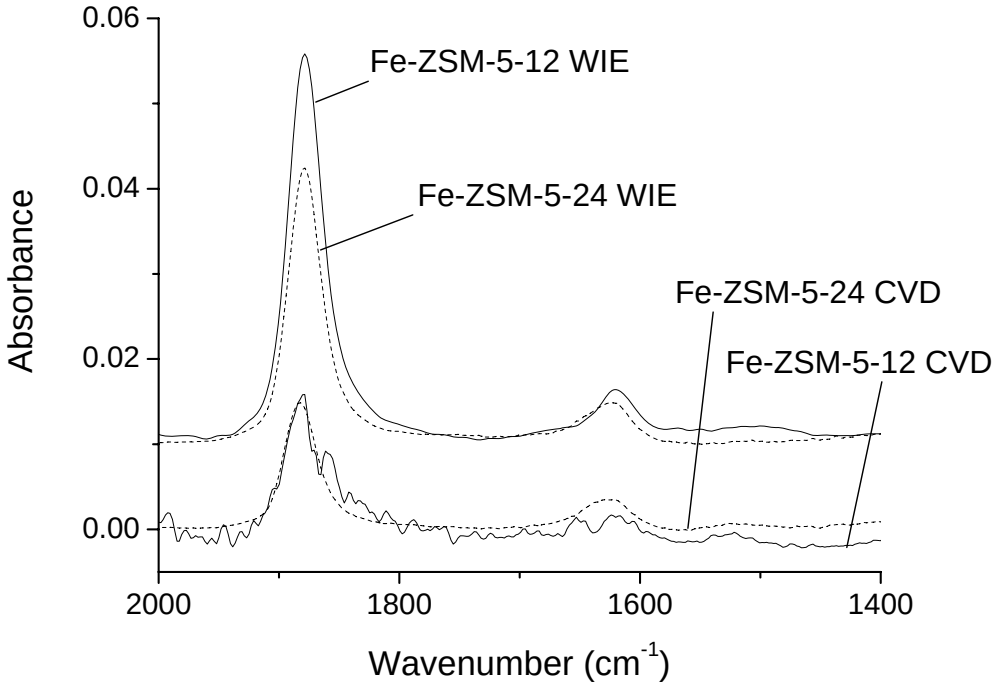

Figure 21 IR spectra after 30 min in 3000 ppm N_2O + 800 ppm NO at 573 K.

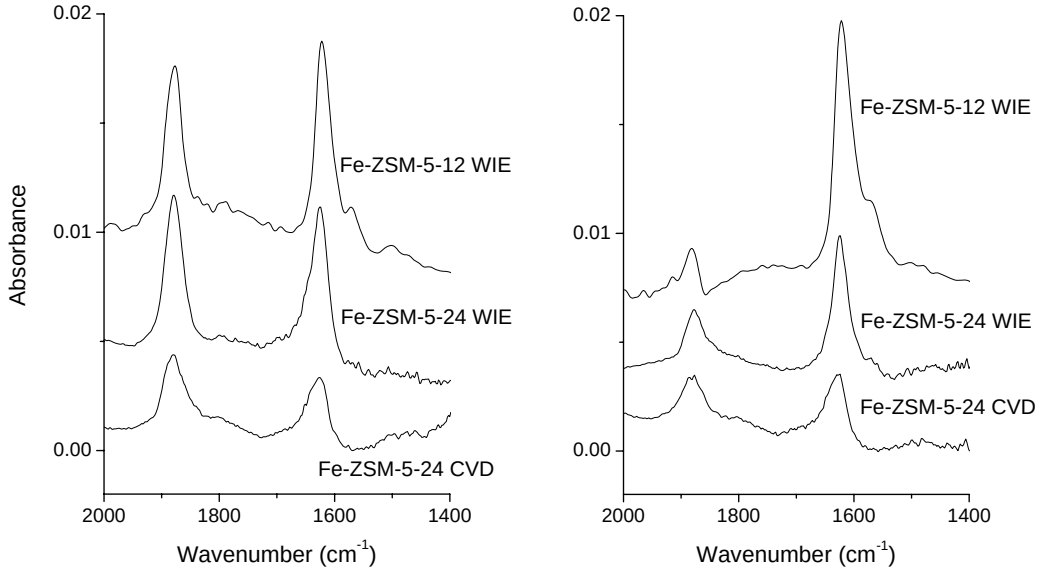

Figure 22 IR spectra after 30 min in 3000 ppm N_2O + 800 ppm NO at (a) 623 K and (b) 648 K.

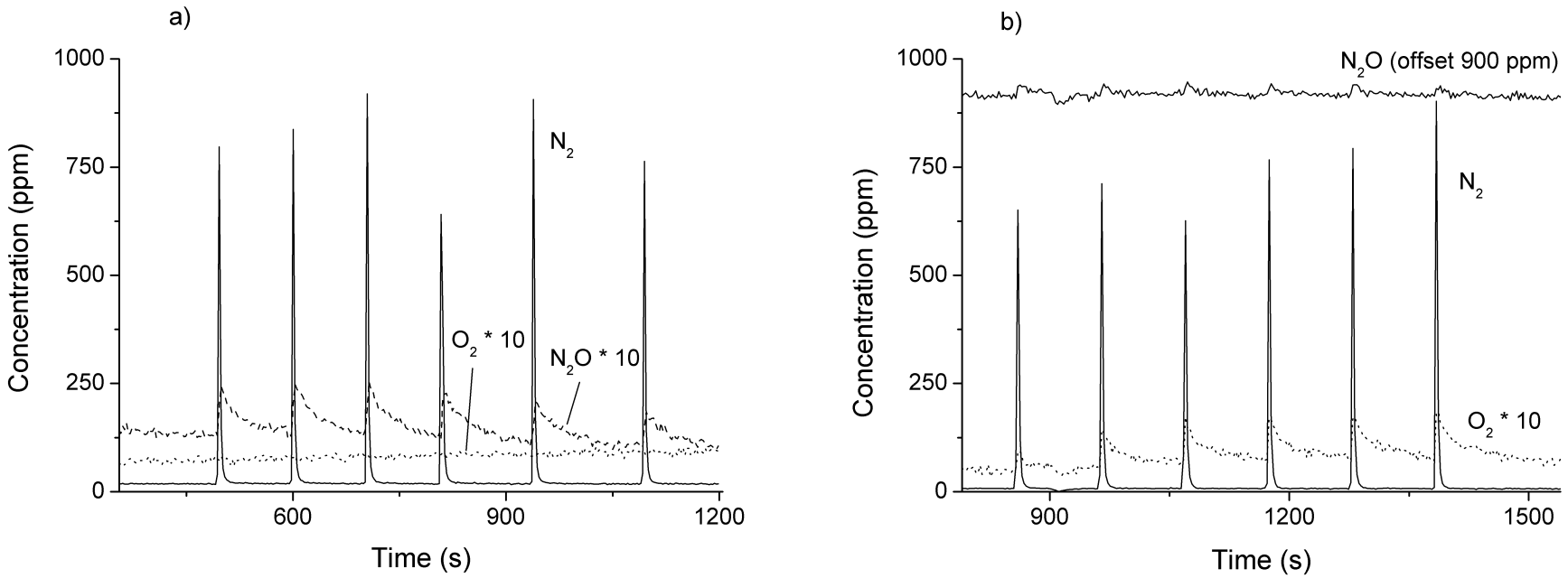

Figure 23 Pulses of 5000 ppm N_2O into a flow of 800 ppm NO at (a) 648 K and (b) 673 K. Fe-ZSM-5-12 WIE, GHSV = 30000 h^{-1}.

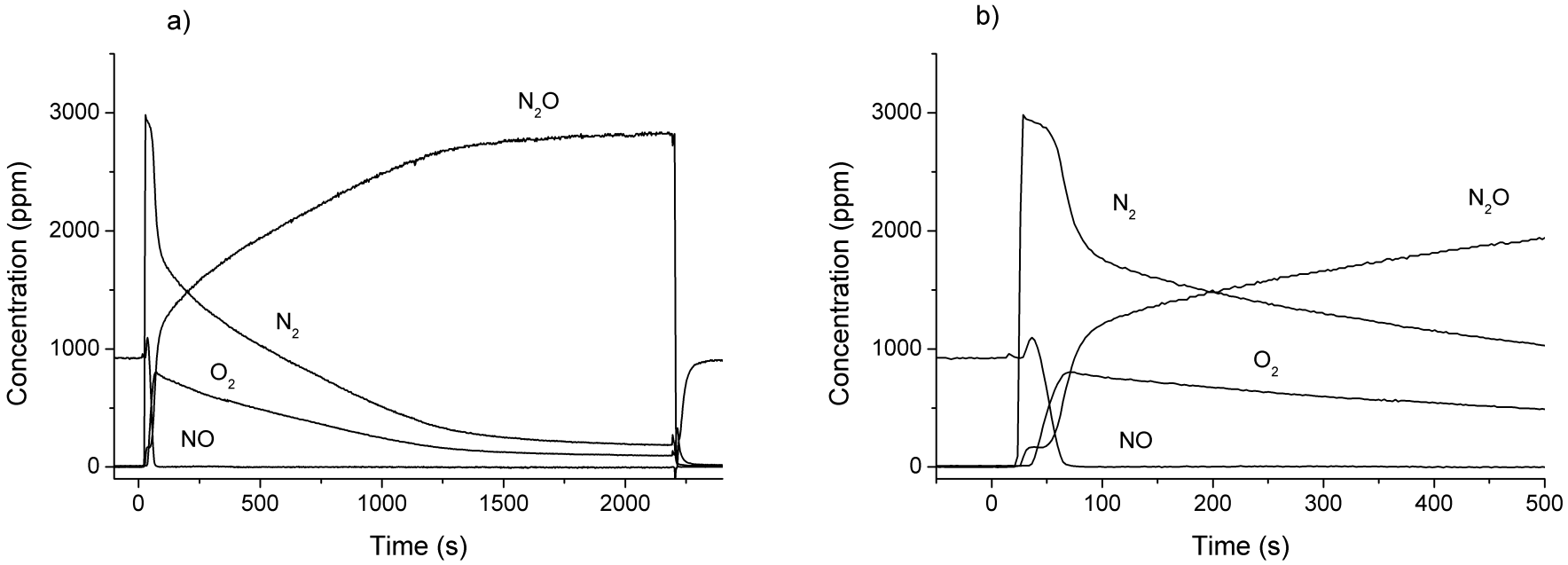

Figure 24 (a) Step from 800 ppm NO to 3000 ppm N_2O in He at 648 K and step back to NO. (b) Zoom of the first 500 s after the step. Fe-ZSM-5-12 WIE, GHSV = 30000 h^{-1}.

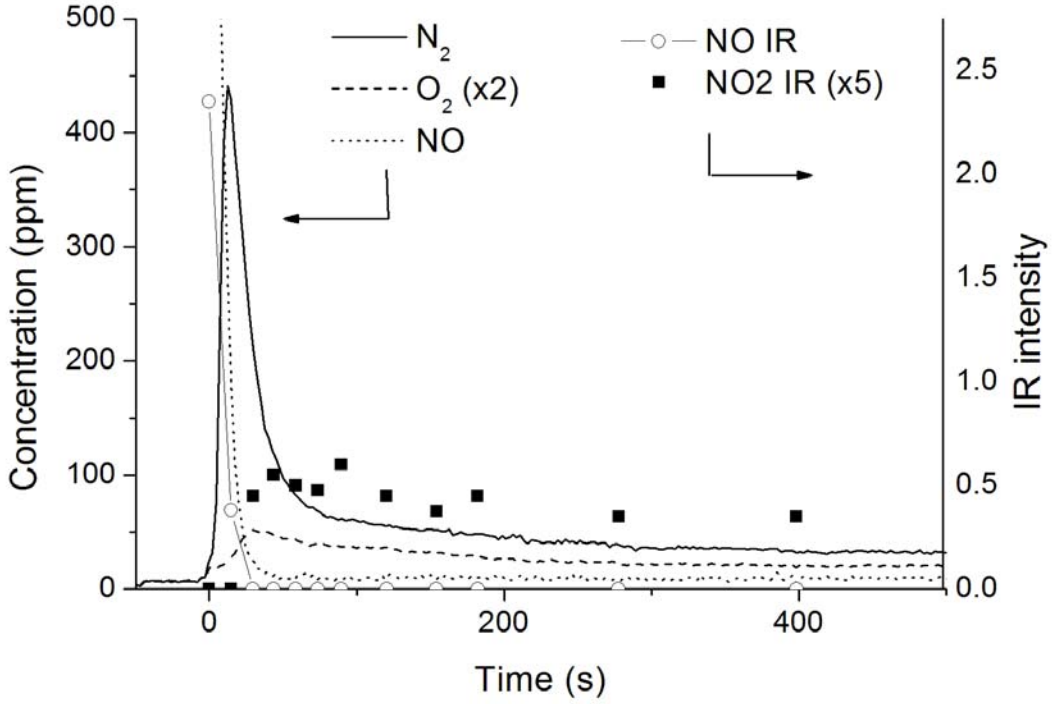

Figure 25 Step from 800 ppm NO to 3000 ppm N_2O in He at 648 K in the IR reactor. Intensity of the nitrosyl band (circles) and of the NO_2 band (x 5, squares) on right axis. Gas phase concentration of N_2 (solid), NO (dotted), and O_2 (x 2, dashed). Fe-ZSM-5-12 WIE, GHSV ~120000 h^{-1} .

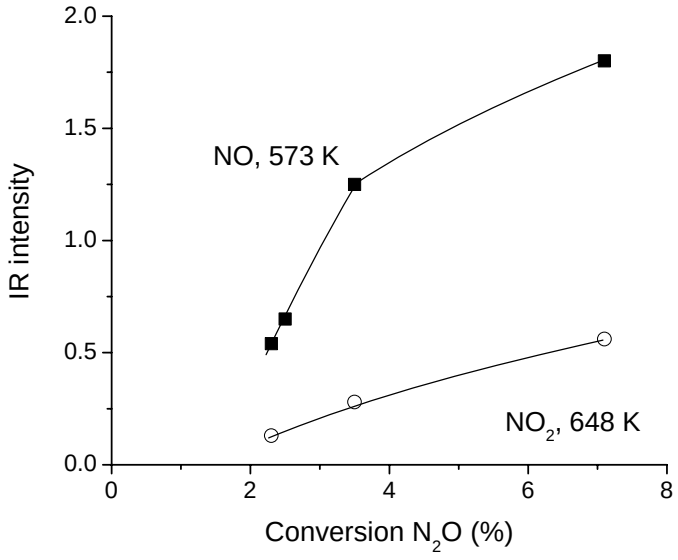

Figure 26 Intensity of the nitrosyl band at 1880 cm^{-1} at 573 K and of the nitro band at 1625 cm^{-1} at 684 K vs. the N_2O conversion at 648 K (in the IR reactor, i.e. at GHSV ~ 120000 h^{-1}).

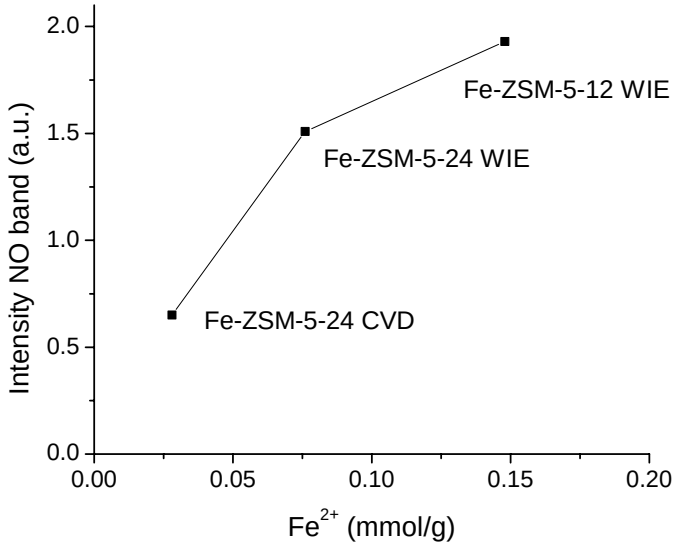

Figure 27 Normalized intensity of the NO band at 1880 cm^{-1} obtained in the IR experiments at 573 K (normalized by thickness of pellet) vs. concentration of Fe^{2+} sites (values derived from Table 3, 648 K).

References:

1 J. T. Houghton, IPCC 3rd assessment report, 2001 (http://www.ipcc.ch/pub/reports.htm).

2 Y. Li, J. N. Armor, Appl. Catal. B 1 (1992) L21.

3 G.Centi, A. Galli, B. Montanari, S. Perathoner, A. Vaccari, Catal. Today 35 (1997) 113.

4 G. Centi, S. Perathoner, F. Vazzana, M. Marella, M. Tomaselli, M. Mantegazza, Adv. Environ. Res. 4 (2000) 325.

5 F. Kapteijn, G. Marban, J. Rodriguez-Mirasol, J. A. Moulijn, J. Catal. 167 (1997) 256.

6 C. Sang, C.R.F. Lund, Catal. Lett. 73 (2001) 73.

7 G. Mul, J. Perez-Ramirez, F. Kapteijn, J. A. Moulijn, Catal. Lett. 77 (2001) 7.

8 J. Perez-Ramirez, F. Kapteijn, G. Mul, J. A. Moulijn, J. Catal. 208 (2002) 211.

9 B. Moden, P. Da Costa, B. Fonfe, D. K. Lee, E. Iglesia, J. Catal. 209 (2002) 75.

10 B. Moden, P. Da Costa, D. K. Lee, E. Iglesia, J. Phys. Chem. B 106 (2002) 9633.

11 J. A. Z. Pieterse, S. Booneveld, R. W. van den Brink, Appl. Catal. B 51 (2004) 215.

12 H. Y. Chen, W. M. H. Sachtler, Catal. Today 42 (1998) 73.

13 P. K. Roy, G. D. Pirngruber, J. Catal. 227 (2004) 164.

14 G. Lehmann, Zeitschrift f. Phys. Chem. Neue Folge 72 (1970) 279.

15 J. Perez-Ramirez, J. C. Groen, A. Brückner, M. S. Kumar, U. Bentrup, M. N. Debbagh, L. A. Villaescusa, J. Catal. 232 (2005) 318.

16 P. Marturano, L. Drozdova, G. D. Pirngruber, A. Kogelbauer, R. Prins, Phys. Chem. Chem. Phys. 3 (2001) 5585.

17 R. Brosius, D. Habermacher, J. A. Martens, L. Vradman, M. Herskowitz, L. Capek, Z. Sobalik, J. Dedecek, B. Wichterlova, V. Tokarova, O. Gonsiorova, Topics Catal. 30/31 (2004) 333.

18 A. Zecchina, S. Bordiga, G. Spoto, L. Marchese, G. Petrini, G. Leofanti, M. Padovan, J. Phys. Chem. 96 (1992) 4991.

19 J. Dedecek, B. Wichterlova, J. Phys. Chem. B 101 (1997) 10233.

20 S. C. Larsen, A. Aylor, A. T. Bell, J. A. Reimer, J. Phys. Chem. 98 (1994) 11533.

21 P. Marturano, L. Drozdova, A. Kogelbauer, R. Prins, J. Catal. 192 (2000) 236.

22 A. A. Battiston, J. H. Bitter, F. M. F. de Groot, A. R. Overweg, O. Stephan, J. A. van Bokhoven, P. J. Kooyman, C. van der Spek, G. Vanko, D. C. Koningsberger, J. Catal. 213 (2003) 251.
23 K. I. Hadjiivanov, Catal. Rev. Sci. Eng. 42 (2000) 71.
24 K. Nakamoto, Infrared and Raman Spectra of Inorganic and Coordination Compounds, Part B: Applications in coordination, Organometallic and Bioinorganic Chemistry, 5th ed., John Wiley & Sons, Inc., New York, 1997.
25 L. J. Lobree, I. C. Hwang, J. A. Reimer, A. T. Bell, Catal. Lett. 63 (1999) 233.
26 K. Hadjiivanov, J. Saussey, J. C. Lavalley, Catal. Lett. 52 (1998) 103.
27 B. R. Wood, J. A. Reimer, A. T. Bell, M. T. Janicke, K. C. Ott, J. Catal. 225 (2004) 300.
28 S. Kameoka, T. Nobukawa, S. Tanaka, S. Ito, K. Tomishige, K. Kunimori, Phys. Chem. Chem. Phys. 5 (2003) 3328.
29 E.J.M. Hensen, Q. Zhu, R.A.J. Janssen, P.C.M.M. Magusin, P.J. Kooyman, R.A. van Santen, J. Catal. 233 (2005) 123.
30 M. V. Konduru, S. S. C. Chuang, J. Phys. Chem. B 103 (1999) 5802.
31 M. V. Konduru, S. S. C. Chuang, J. Catal. 196 (2000) 271.
32 G. D. Pirngruber, J. Catal. 219 (2003) 456.
33 T. Nobukawa, M. Yoshida, K. Okumura, K. Tomishige, K. Kunimori, J. Catal. 229 (2005) 374.
34 P. Da Costa, B. Moden, G. D. Meitzner, D. K. Lee, E. Iglesia, Phys. Chem. Chem. Phys. 4 (2002) 4590.
35 A. A. Battiston, J. H. Bitter, F. M. F. de Groot, A. R. Overweg, O. Stephan, J. A. van Bokhoven, P. J. Kooyman, C. van der Spek, G. Vanko, D. C. Koningsberger, J. Catal. 213 (2003) 251.
36 E. J. M. Hensen, Q. Zhu, M. Hendrix, A. R. Overweg, P. J. Kooyman, M. V. Sychev, R. A. van Santen, J. Catal. 221 (2004) 560.
37 G. D. Pirngruber, P. K. Roy, N. Weiher, J. Phys. Chem. B 108 (2004) 13746.
38 G. Berlier, G. Spoto, G. Ricchiardi, S. Bordiga, C. Lamberti, A. Zecchina, J. Mol. Catal. A 182 (2002) 359.
39 L. J. Lobree, I. C. Hwang, J. A. Reimer, A. T. Bell, J. Catal. 186 (1999) 242.
40 G. Mul, J. Perez-Ramirez, F. Kapteijn, J. A. Moulijn, Catal. Lett. 80 (2002) 129.
41 H. Y. Chen, T. Voskoboinikov, W. M. H. Sachtler, J. Catal. 180 (1998) 171.
42 E. M. El-Malki, R. A. van Santen, W. M. H. Sachtler, Microporous Mesoporous Mat. 35-36 (2000) 235.

43 E. M. El-Malki, R. A. van Santen, W. M. H. Sachtler, J. Catal. 196 (2000) 212.

44 B. R. Wood, J. A. Reimer, A. T. Bell, J. Catal. 209 (2002) 151.

45 C. Sang, B. H. Kim, C. R. F. Lund, J. Phys. Chem. B 109 (2005) 2295.

46 G. D. Pirngruber, M. Luechinger, P. K. Roy, A. Cecchetto, P. Smirniotis, J. Catal. 224 (2004) 429.

47 G. D. Pirngruber, P. K. Roy, Catal. Lett. 93 (2004) 75.